CrossMark

Numerical analysis of the Black Sea currents and mesoscale eddies in 2006 and 2011

Sergey Germanovich Demyshev [1] · Olga Alekseevna Dymova [1] ⓘD

© Springer-Verlag GmbH Germany, part of Springer Nature 2018

Abstract

Two prognostic experiments taking into account real atmospheric forcing for 2006 and 2011 were carried out based on the eddy-resolving numerical model with a horizontal resolution of 1.6 km for the Black Sea. The main dynamic features such as the Rim Current, the Sevastopol, and Batumi anticyclones are reproduced in both experiments. The model results are confirmed via observation data. We accomplished the analysis of simulated circulation and energetics. The results demonstrate that both the vertical viscosity and vertical diffusion along with the energy inflow from the wind have been the main contributors to the annual and seasonal budgets of kinetic and potential energies of the Black Sea circulation. It is shown that two regimes of the Black Sea general circulation are implemented depending on a magnitude of wind contribution to the kinetic energy in winter. Intensive mesoscale eddy formation was observed along the Anatolian, Caucasian, and Crimean coasts. The analysis of the Black Sea circulation and eddy energetics allowed us to conclude that the generation and development of the mesoscale coastal eddies is associated with the barotropic instability in case of intensive coastal currents and is associated with both the barotropic and baroclinic instability in case of weak coastal currents.

1 Introduction

Presently, great interest is focused on the study of mesoscale variability of currents in the seas and oceans. Primarily this happens due to the importance of eddies for transport of mass, energy, heat, and salt from the coastal to deep-water parts of the basin in semi-enclosed seas. Such a problem is especially significant for the Black Sea, where the central part of the sea and its periphery are divided by the Rim Current.

During our earlier investigations, we performed a review of various literature sources devoted to the study of eddies in oceans

and seas. Here we do not aim to describe all the natural reasons of the eddy formation in the oceans; however, we would like to mention four main, in our opinion, generation mechanisms:

1. Eind influence (e.g., Kersalé et al. 2011; Liang et al. 2012)
2. Barotropic instability and/or baroclinic instability of the currents (e.g., Cushman-Roisin et al. 2007; Chen et al. 2012; Zhang et al. 2013)
3. Fluxes of impulse and mass through lateral boundaries such as estuaries and straits (e.g., Schaeffer et al. 2011; Prants et al. 2017)
4. Topographic and orographic effects (e.g., Schaeffer et al. 2011; Ponomarev et al. 2011)

To study the reasons of the eddy formation and evolution, there is an effective method of calculation and analysis of the equations of the changes in kinetic (KE) and potential (PE) energies. The terms of these equations indicate the work of the main forces. In the original study (Robinson et al. 1977), the research results of the integral energy characteristics of circulation in the idealized ocean are presented and the estimations describing contributions due to wind and thermal effects in eddies energy and mean current energy are given. The role

---

Responsible Editor: Sergey Prants

This article is part of the Topical Collection on the *International Conference "Vortices and coherent structures: from ocean to microfluids," Vladivostok, Russia, 28–31 August 2017*

✉ Sergey Germanovich Demyshev
demyshev@gmail.com

1   Marine Hydrophysical Institute of RAS, 2, Kapitanskaya Street, Sevastopol, Russia 299011

of barotropic and baroclinic instability in the formation of the eddy energy is shown.

The influence of horizontal resolution on the description accuracy of direct and inverse energy cascades in numerical models is studied in Kjellsson and Zanna (2017). The authors demonstrate approaches for parameterization of mesoscale processes which permit to avoid underestimations in the KE and PE budgets. Numerical estimations of seasonal variability of eddy kinetic energy (EKE) in the Global Ocean are presented in Rieck et al. (2015). It is obtained that seasonal increase in thermal fluxes from the atmosphere causes intensification of mesoscale variability in the velocity field near the ocean surface. Shang et al. (2013) estimate the spatial distribution of sources and sinks of eddy energy for actually observed mesoscale structures based on the analysis of the average EKE distribution calculated according to satellite altimetry.

Assessments of the eddies energy and the mean currents energy are also performed for the Black Sea by the simulation results and observations. Oguz et al. (1995) study the relative contributions of wind influence, the thermohaline surface fluxes, the river discharge, and the inflow/outflow through the Bosphorus to the formation of the Black Sea circulation based on of numerical experiments. It is shown that intensification of mesoscale dynamics in coastal zones is a consequence of dynamic evolution of the Rim Current. The results of Rachev and Stanev (1997) demonstrate that for the Black Sea, the seasonal variability of the density field has the main effect on the coastal anti-cyclone generation due to nonlinear dynamics of waters. In Trukhchev et al. (1999), the velocity fields on the western Black Sea shelf are reconstructed using a high-resolution model (1 mile). It is shown that the small-scale eddy structure of coastal currents agrees qualitatively and quantitatively with the observation data. The mean flow kinetic energy (MKE) and the EKE are calculated in Menna and Poulain (2014) using the drifter and altimetry data. Analysis shows that mesoscale eddies near the Anatolian coast and in the North-East of the Black Sea can significantly increase their kinetic energy due to interaction with each other. It leads to the generation of new quasi-constant mesoscale eddies. The energy balances of semi-enclosed seas (including the Black Sea) are calculated in Cessi et al. (2014) and it is shown that the buoyancy force is one of the main factors for the formation of mesoscale dynamics in semi-enclosed seas. The research of geometrical, temporal, statistical, and energetic characteristics of eddies in the Black Sea is carried out in Kubryakov and Stanichny (2015a) based on altimetry satellite observations.

The majority of modern works devoted to the numerical analysis of the ocean energy cycle the researchers calculate the KE and PE of currents and eddies based on allocating the time-mean values of velocity and density and their

deviations from the mean (time-varying fluctuations) (for example, see Von Storch et al. 2012). Similarly, the rates of energy conversion and energy sources due to external influence are estimated. However, it is assumed that the density anomaly is a deviation from the predefined reference density and there is not equation for the available potential energy in the finite-difference shape which obtained as an exact consequence of discrete formulation of the problem. A more correct way is to obtain finite-difference analogues of differential energy equations based on discrete equations of the circulation model. In this case, the calculated three-dimensional energy fields will correspond exactly to the change of hydrological fields. Such equations were obtained earlier in Demyshev (2004) and will be used in this work for analysis of the circulation energetics. The eddy energy will be studied based on the equations of work (Von Storch et al. 2012).

Earlier in Demyshev (2004), the energy of the Black Sea climatic circulation was investigated and five energy active zones were determined: along the dump of depths in the North-Western shelf area, near the Western part of the Anatolian coast, in the South-Western part of the sea, near the central part of the Caucasus coast, and near Eastern Crimea. The main balances of forces responsible for the formation of large-scale climatic circulation are calculated. However, it was difficult to clearly distinguish the physical mechanisms of formation of the seasonal circulation variability, because the assimilation terms were included in the model equations, which added a significant contribution to the force balance.

In present work, the real atmospheric forcing is taken into account, horizontal resolution is improved, and the Mellor-Yamada turbulence closure model 2.5 is used to describe a vertical mixing (Mellor and Yamada 1982). The results of the "MyOcean" project (Demyshev et al. 2010) show that there is a substantial difference in the currents dynamics for different years. The main source of the currents KE in the Black Sea is wind and the strength of the autumn-winter wind activity determines the structure of the basin circulation (Zatsepin et al. 2010). QuickSCAT (https://podaac-opendap.jpl.nasa.gov/opendap/allData/ccmp/L3.0/flk/2006/01/contents.html) observations show that extremely strong winds with velocities of more than 20 m/s acted over the Western part of the sea in January 2006. It enhanced the surface currents velocities up to more than 1 m/s and storm waves up to 6 m high emerged in the South-Western part of the sea (Kortcheva et al. 2009). The analysis of the wind fields in different time periods allowed us to choose a year in which winter wind influence was significantly weaker than in 2006. Therefore, we expected that the circulation structure will be different. So, the goal of this work was to evaluate the influence of different physical processes on the variability of the basin-scale circulation and mesoscale

eddies in the Black Sea based on the analysis of KE and PE budgets.

Section 2 describes model configuration and experiment setting. In Section 3, we demonstrate results of validation and calibration of the modeling thermohaline fields. In Section 4, we submit equations for calculating the components of KE and PE budgets. Section 5 presents the modeling results. Here we analyzed integral mean currents and eddy energy balances and the contributions of physical processes which form it. Mesoscale variability of the Black Sea circulation is considered in Section 5, too. The main conclusions are discussed in Section 6.

2 Model and the experiment setting

Numerical experiments were carried out based on the eddy-resolving model of Marine Hydrophysical Institute of RAS (MHI model) (Demyshev 2012). The complete equations of ocean thermohydrodynamics were implemented in the MHI model. The equations were written in Boussinesq, hydrostatics, and seawater incompressibility approximations. The sea level was calculated assuming the linearized kinematical condition. Density depended nonlinearly on temperature and salinity (Mamaev 1963). Vertical mixing was parameterized by the Mellor-Yamada turbulence closure model of level 2.5 (Mellor and Yamada 1982).

We set the tangential wind stress, full heat fluxes, precipitation, and evaporation obtained from the atmospheric reanalysis data as boundary conditions on the sea surface. The river discharges of Danube, Dnieper, Dniester, Rioni, Kizilirmak, Yeshilirmak, and Sakarya and water exchanges through the Bosphorus and the Kerch Straits were counted in the model. The rivers volume transport corresponded to monthly average climate data (Project 1991). The Black Sea bottom configuration was built by linear interpolation from the 5-km-resolution topography obtained from the MHI database (Khaliulin et al. 2016). The MHI model had a horizontal resolution of 1.6 km on both geographical coordinates and 27 vertical z-levels were set. Axes X and Y were directed to the East and to the North, respectively, and axis Z was directed from surface to the bottom. The baroclinic Rossby radius of deformation in the Black Sea coastal zones varied from 7 to 20 km depending on the shelf depth. Thus, the spatial resolution of the MHI model was smaller than the Rossby radius of deformation and we could reconstruct the mesoscale variability. Horizontal viscosity in momentum equations and horizontal diffusion in heat-salt transport equations were calculated by the fourth-order operator with coefficients $\nu_H = 10^8$ m^4 s^{-1} and $\kappa_H = 5 \cdot 10^8$ m^4 s^{-1}, respectively. The fields of level, temperature, salinity, and horizontal velocity components were set at the initial time.

Two numerical experiments were carried out with different atmospheric forcing. The wind stress was directly taken into account as a surface boundary condition in the movement equations and equations of the turbulence closure model. Therefore, the selection of the forcing was determined by the intensity of the wind. In our experiments, the components of wind stress vector were obtained by the ratio $\overrightarrow{\tau} = \rho C_d \left| \overrightarrow{V} \right| \overrightarrow{V}$ (Volcinger and Piaskovski 1968), where ρ is air density, C_d seawater resistance coefficient, and $\overrightarrow{V}$ absolute wind velocity on 10 m. We chose 2 years, 2006 and 2011, for which winter total values of wind stress for the former are twice as large as for the latter: 130.6 N and 72.3 N, respectively. We consider hydrological winter to be from January till March. Histograms of occurrence of wind directions and magnitudes for the winter months of 2006 and 2011 are presented in Fig. 1. Percentage of occurrence of wind directions is calculated according to wind data at each model grid point during the winter months; color represents the wind stress magnitude (10^{-5} N). It is seen that the North-Eastern winds prevailed in the winters of 2006 and 2011, but in 2006, the winds were more intense. The maximum wind stresses were equal $7.63 \cdot 10^{-5}$ N (≈ 28 m/s) on January 24, 2006 and $4.65 \cdot 10^{-5}$ N (≈ 17.8 m/s) on February 19, 2011. Generally, there were more strong winter winds (more than 10^{-5} N) in 2006 than in 2011. In summer, the total wind force decreased to 66.4 N in 2006 and 42.1 N in 2011; the storms were shorter and weaker than in winter. For example, compare the storms on July 3, 2006 and on June 27, 2011, when the wind velocities reached 15 m/s.

In experiment 1 (Exp.1), atmospheric fluxes obtained from the ALADIN reanalysis data with a resolution of 0.25° (Farda et al. 2010) were set at the sea surface. Since there were no initial data of a sea level, temperature, salinity, and currents on January 1, 2006, we used climatic hydrophysical fields (Demyshev et al. 2009) corresponding to January 1. The procedure of a quasi-geostrophic adjustment was applied to agree climatic fields with atmospheric forcing. For this purpose, we integrated the model equations for 4 days of model time under constant boundary conditions corresponding to January 1, 2006 according to ALADIN. Then, the obtained fields were used as a starting point for Exp.1, which was run for the period of January 1–December 31, 2006.

In experiment 2 (Exp.2), we used the SKYRON reanalysis data with a resolution of 0.1° (Kallos et al. 1997) as boundary conditions on the sea surface. Initial fields were prepared on the basis of the Black Sea hydrophysical field reanalysis data (http://marine.copernicus.eu/services-portfolio/access-to-products/). The quasi-geostrophic adjustment procedure was also used here. The simulation time in Exp.2 corresponded to the period of January 1–December 31, 2011.

In both experiments, the sea surface temperature was assimilated on the upper model horizon each day. For the first
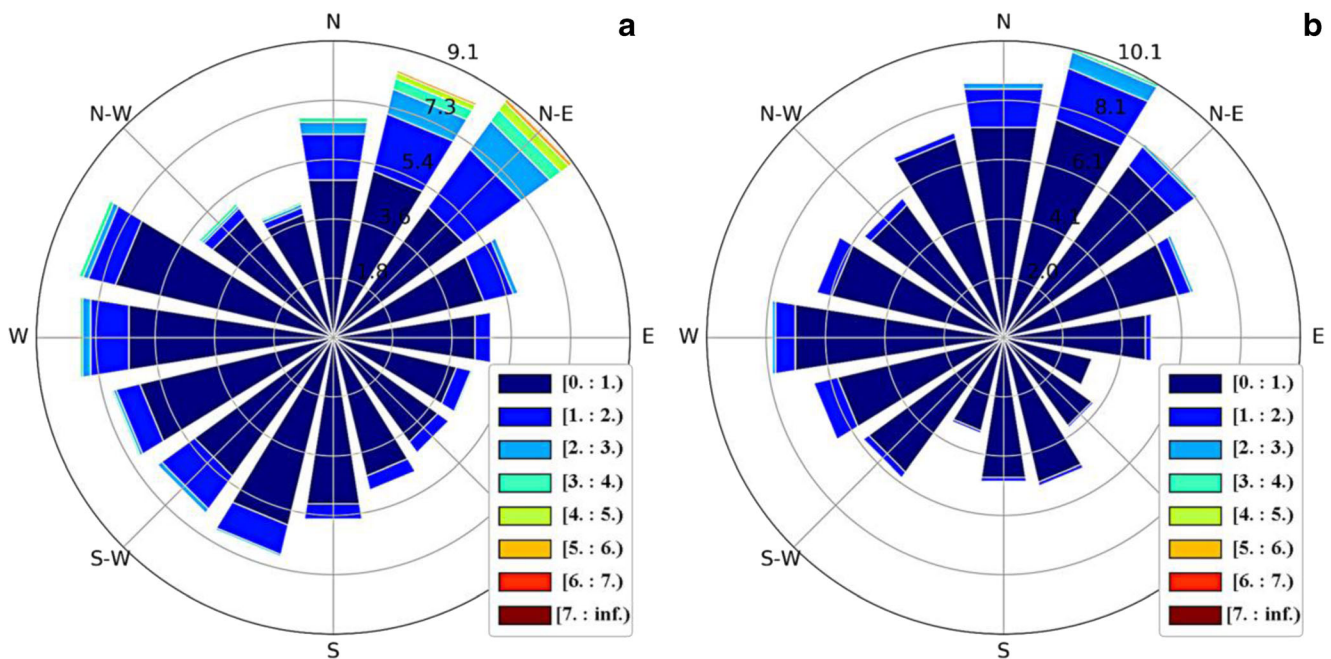
Fig. 1 Histograms of the directions and wind stress magnitude (10^{-5} N) bands, representing the occurrence (in percentage) of winds with the given direction and magnitude, estimated for the Black Sea area from January till March: in 2006 (**a**) and 2011 (**b**). Data were calculated from the atmospheric forcing wind velocity and direction at the height of 10 m

experiment, it was obtained from the NOAA satellite data (http://dvs.net.ru/mp/data/200601bs_sst.shtml) and for the second one the SKIRON data. It is important to note that all input data had different spatial resolution, so all arrays were linearly interpolated to the nodes of our model grid (1.6 km horizontally) before the starting of calculations. The horizontal viscosity and diffusion coefficients were the same in both experiments. Three-dimensional fields of temperature, salinity, current velocities, and fields of the energy budget components for each day of 2006 and 2011 were obtained as a result of the experiments.

3 Validation of the results

Calibration and further validation of the MHI model was accomplished in the framework of the "MyOcean" project (Demyshev et al. 2010). As an example, we present here the validation of modeling results for 2006. Figure 2a shows the positions of conductivity, temperature, and depth (CTD) stations on standard sections at the polygon of the Southern Branch of the P.P. Shirshov Institute of Oceanology (Gelendzhik, Russia). We used the data obtained from three cruises (97, 101, and 103) from May till July 2006. This makes 52 stations in total. The CTD profiles were obtained for the coastal and abyssal parts of the sea, so we were able to estimate the accuracy of modeling for both zones. Note that the number of profiles was less than the number of stations because there were interruptions at the stations no. 2453-2455,

no. 2501, and no. 2527-2536 (Fig. 2a). Figure 2b, c illustrates the profiles of deviation between in situ and modeling temperature and salinity at model z-levels for every third station. The black line marks the deviation averaged over all profiles.

The model reproduced all qualitative features of the temperature field variability during the warm period of 2006. We observed the intense heating of the sea surface in spring which entailed an increase in temperature gradient in the layer from the surface to the upper boundary of the Cold Intermediate Layer (CIL). The core of the CIL was detected into all profiles at the depths of 30–100 m. The analysis of the model data showed that the upper boundary of the CIL was placed 5 m deeper than under observations. Therefore, the model temperature exceeded in situ data at the station nos. 2509, 2519, 2538, and 2546 due to vertical displacement of the thermocline depth in the 10–15-m layer (Fig. 2b). Underestimation of temperature was also observed at coastal station no. 2456-2460. These errors might be caused by various reasons, including the quality of atmospheric forcing, the correctness of sub-grid processes parameterization, and the accuracy of finite-difference approximations. Below 200 m deep, the model temperature differs from the measured one by a few hundredths of a degree.

A good agreement between the salinity field and the measurement data in the upper 50-m layer was observed. The greatest deviations (about 1‰) from the in situ measurements occurred at station nos. 2460, 2506, 2509, 2515, and 2518 in the layer of 50–150 m (Fig. 2c). These stations were located over the depths dump (no. 2460, 2506), as well as over the

Fig. 2 Fragment of the Black Sea bathymetry map (blue line, m) and numbers of CTD stations (**a**), the deviation profiles of simulated temperature (**b**), and salinity (**c**) from observations on each third station. Black line denotes the deviation profile averaged over all illustrated stations
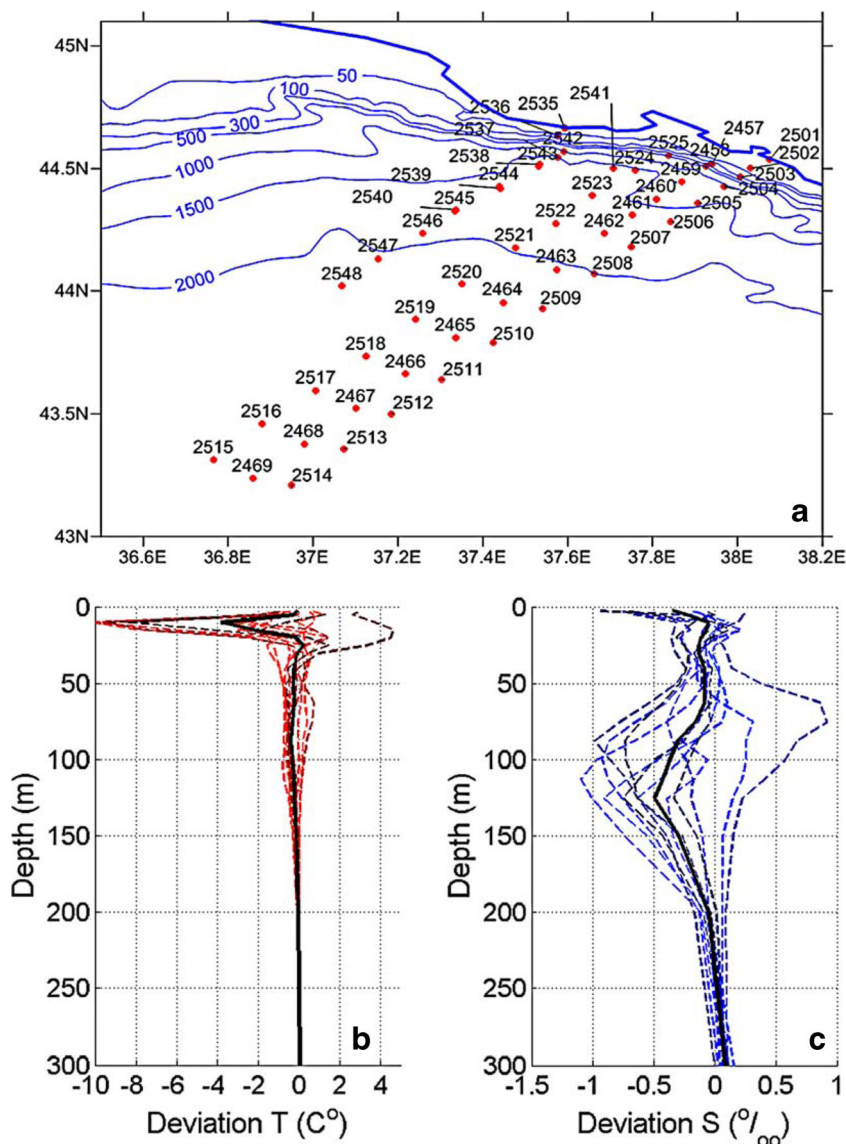

deep-water part (nos. 2509, 2515, 2518) of the sea. Intensive restructuring of the density field in the up 200-m layer was observed in spring under the influence of the atmospheric forcing. Therefore, an underestimation of the formation mechanisms of the seasonal halocline led to relatively large errors at these depths. There is a good quantitative correspondence between the observed and the model salinity for all stations below 200 m.

Model velocity fields reconstruct the main features of circulation. General basin-scale cyclonic gyre, so-called the Rim Current, covers the deep part of the Black Sea. The Rim Current has a size of about 10^3 km and the mean midstream velocity of about 40 cm/s. Trajectory of drifter no. 40414 which worked in the Black Sea from July till November 2006 (Motyzhev et al. 2016) is presented in Fig. 3a. As seen, the drifter moved alongside depth dump (exclude the eastern

sea part). We estimated a Lagrangian velocity of the drifter and compared with model data in the same points. Model current velocities are close to them (see Fig. 3b).

The Sevastopol (SA) and Batumi (BA) anticyclones are most intensive and biggest mesoscale eddies in the Black Sea. Existence of these anticyclones is confirmed via drifter and satellite data (Zhurbas et al. 2004, Menna and Poulain 2014, Kubryakov and Stanichny 2015b, Motyzhev et al. 2016). They can reach sizes of about 150 km and more the orbital velocities of about 50–60 cm/s and more. Archive of the Black Sea satellite information from 2004 till present time is freely available on Marine Portal of MHI (http://dvs.net.ru/mp/index.shtml). As an example, we demonstrate model velocity field on December 16, 2006 and the satellite sea surface temperature on the same date in Fig. 4. The warm water domains (denoted red line circle) correspond to the SA

Fig. 3 Trajectory of drifter no. 40414 (**a**) and velocities along the drifter track (**b**). Blue line denotes Lagrangian velocity of the drifter. Red line denotes simulated surface current velocity
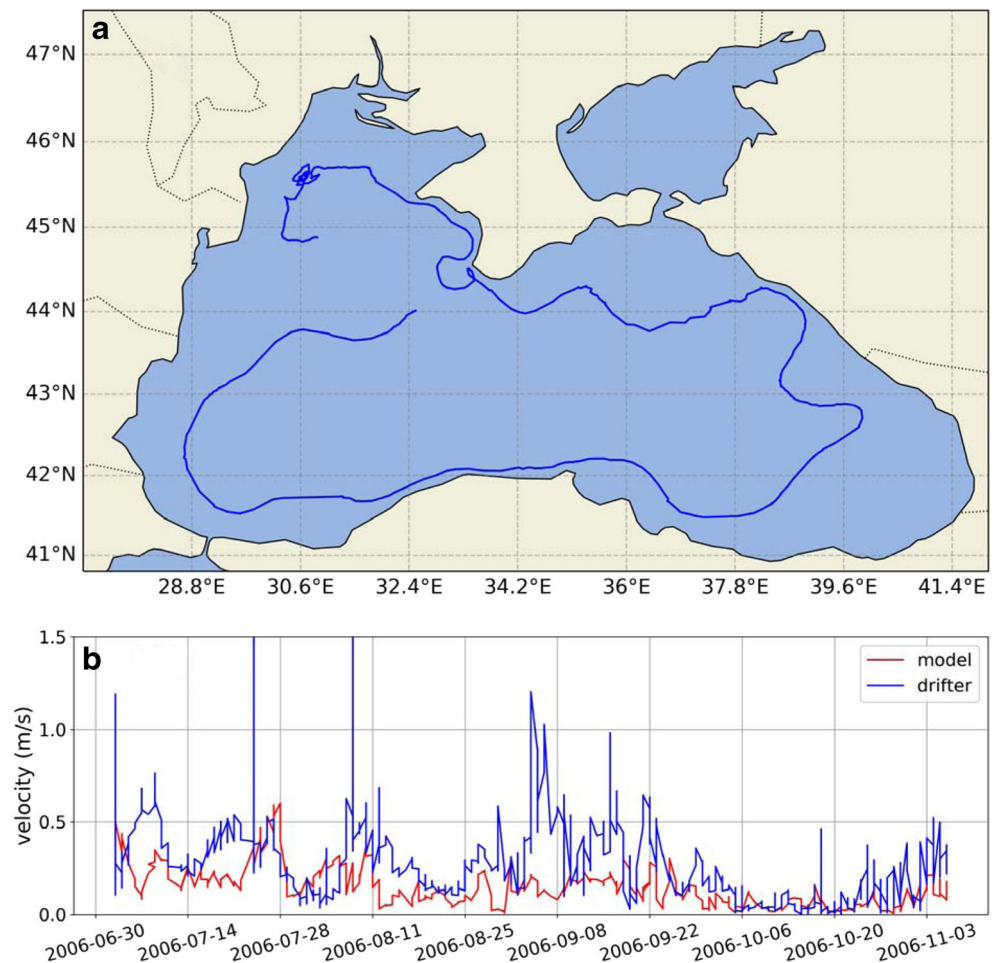
and BA (Fig. 4a) and the anticyclonic eddies are also observed in the model velocity field (Fig. 4b). The BA is quasi-stationary eddy in the South-Eastern part of the Black Sea, usually it is observed from April till November but sometimes its lifetime exceeds 1 year (Kubryakov and Stanichny 2015b). Cyclonic eddy can accompany the BA at the end of year (see in Fig. 4b, blue line circle). The SA is quasi-periodical eddy. It character feature is a movement along continental slope toward the South-West. Analysis of satellite images (Ginzburg et al. 2002) shown that the eddy are generated toward the West from Sevastopol (Fig. 4b) and then are propagated along periphery of the Rim Current. The SA is dissipated near Bulgarian coast after 3–4 months. The model mesoscale variability agrees with estimations obtained by measurements and simulation data (Staneva et al. 2001, Korotenko 2015).

4 Energy equations

The equations of the KE and PE change rates and the specificity of their finite-difference approximation are presented in detail in Demyshev (2004). Let us remind them for better understanding of the text below. Denote KE as $E = \rho_0 \frac{u^2 + v^2}{2}$. We assume that $\rho_0 = 1$ g cm^{-3}. Here and hereafter, u, v, and w are zonal, meridional, and vertical velocity components, p is the pressure, ρ is the density, g is the gravity acceleration, and ν_H and ν_V are the horizontal and vertical viscosity coefficients, respectively. Indexes x, y, z, and t indicate a differentiation with respect to the corresponding parameter. The KE change rate can be written as follows:

$$E_t = -Adv(p) - Adv(E) + P \leftrightarrow E + \tau \rightarrow E$$
$$+ Diss_{ver}(E) + Diss_{hor}(E), \qquad (1)$$

where,

$Adv(p) = (up)_x + (vp)_y + (wp)_z$ is the pressure work
$Adv(E) = (uE)_x + (vE)_y + (wE)_z$ is the advection of KE
$P \leftrightarrow E = \rho g w$ is the buoyancy work
$\tau \rightarrow E = u_0 \tau^x + v_0 \tau^y$ is the wind stress work
$Diss_{ver}(E) = -\nu_V(uu_z + vv_z)_z$

Fig. 4 Remote sensing sea surface temperature (**a**) on December 16, 2006 (available on http://dvs.net.ru/mp/index.shtml). SA, the Sevastopol anticyclone; BA, the Batumi anticyclone. Simulated fields of the surface current velocity (**b**), where red circles denote the anticyclones and blue circle denotes the cyclone
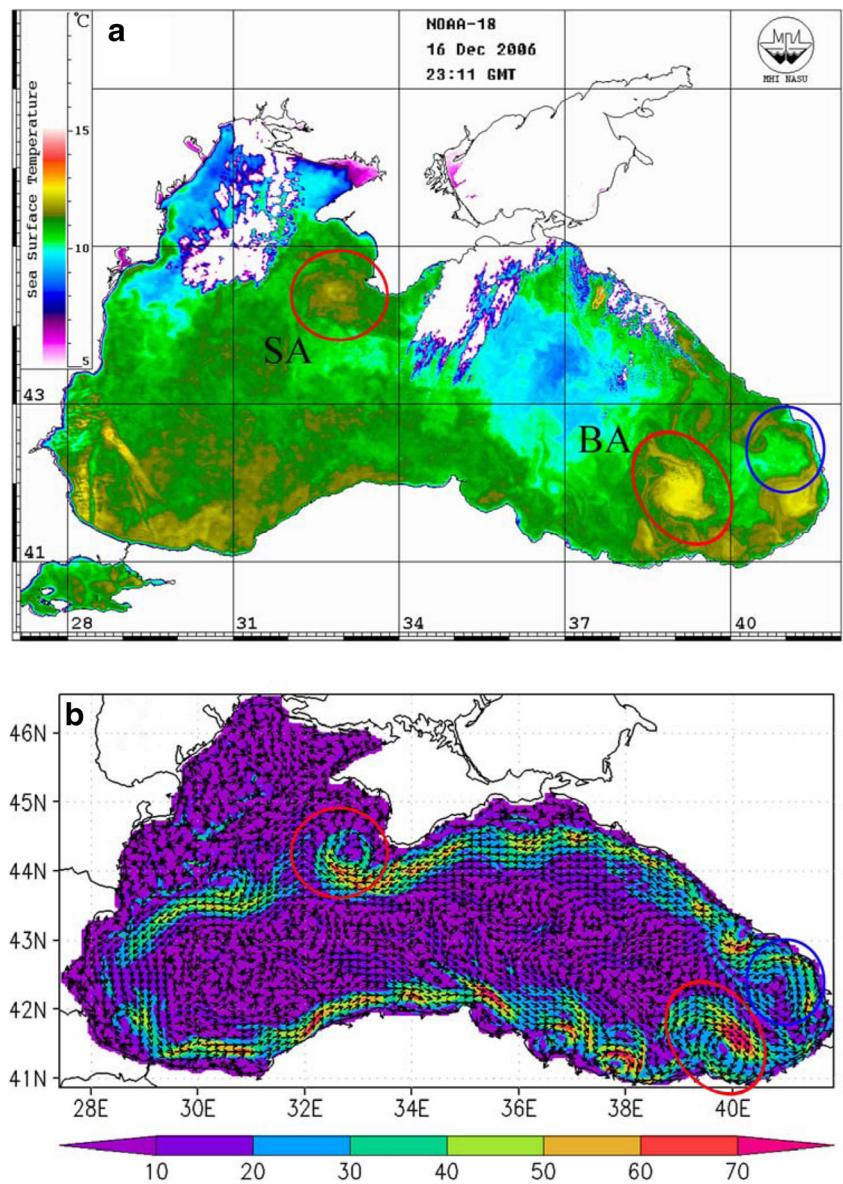
$$Diss_{hor}(E) = -\nu_H[(\Delta u)^2 + (\Delta v)^2]$$

is the work due to vertical internal friction and bottom friction

is the work due to horizontal friction which includes horizontal internal friction and lateral friction, Δ – Laplacian

The equation of the PE change rate has a view of (taking into account that $P = -gz\rho$):

$$P_t = -Adv(P) - P \leftrightarrow E + Diff_{hor}(P) + Fluxes + Diff_{ver}^{in}(P) + \\ + Diff_{ver}^{\rho}(P) + Diff_{ver}^{\kappa_V}(P) + Diff_{ver}^{add}(P),$$

(2)

where,

$Adv(P) = (uP)_x + (vP)_y + (wP)_z$ is the PE advection

$Diff_{hor}(P) = -\kappa_H gz((\nabla^2\rho)^2 - Q^H)$ is the work due to horizontal diffusion of PE

$Fluxes = -gz\kappa_V(\rho)_z|_{z=0}$ is the change of PE due to heat and salt fluxes from the atmosphere through the sea surface

$Diff_{ver}^{in}(P) = -g(\kappa_V z\rho_z)_z$ is the term corresponding to the internal vertical turbulent diffusion

$Diff_{ver}^{\rho}(P) = -g\kappa_V(\rho)_z$ is the term corresponding to the dependence of the density on depth

$Diff_{ver}^{\kappa_V}(P) = -g\rho(\kappa_V)_z$ is the term corresponding to the dependence the vertical diffusion coefficient on depth

$Diff_{ver}^{add}(P) = -gz\kappa_V Q^V$ is the term which appears due to a nonlinear form of the density equation

Here, κ_H and κ_V are the horizontal and vertical diffusion coefficients, respectively; Q^H and Q^V are the terms corresponding to the nonlinear form of the density equation. Below in Section 5, we will consider the densities of KE and PE change in order to analyze the year-mean and the season-mean KE and PE budgets. These variables are derived as volume integrals of the terms of Eqs. (1) and (2): $< \phi >^V = \frac{1}{V}\iiint \phi\, dz dx dy$, where V is a basin volume.

5 Analysis of the modeling results

It is common knowledge (Titov and Savin 2008) that the Black Sea dynamics is characterized by the Rim Current and anticyclonic eddies on its periphery. Classification of the vortex structures is accomplished through evaluating the baroclinic Rossby radius of deformation R_d and the Rossby number Ro, which characterizes the relationship between the inertial force and the Coriolis force (Gill 1982):

$$R_d = \frac{\sqrt{gH(\Delta\rho/\rho)}}{f}, \quad Ro = \frac{U}{Rf}, \qquad (3)$$

where U is the orbital eddy velocity, R is the eddy radius, and f is the Coriolis parameter. If eddies have Ro smaller than 1 and size bigger than R_d, then they are called mesoscale. Calculations and in situ measurements for the Black Sea show that mesoscale eddies are predominately discovered between the Rim Current and the shore over the continental slope. They have an average size of 15–30 km and a lifetime of about 2–3 months (Stanev 1990; Ibraev and Trukhchev 1996). So, we relate these eddies to mesoscale (Chelton 2001). The analysis of the temporal-spatial variability of velocity, density, and energy balance in the vicinity of eddies allowed us to assume that the mechanisms of mesoscale eddies generation in the Black Sea are the baroclinic instability due to the vertical shear of the coastal currents (Dymova 2017).

5.1 Energetics

The volume integrals of the circulation KE and PE components are calculated for each day from Eqs. (1) and (2). The KE change is determined by the pressure work $Adv(p)$, the advection of KE $Adv(E)$, the buoyancy work $P \leftrightarrow E$, and the wind stress work $\tau \rightarrow E$. KE is lost due to the horizontal

$Diss_{hor}(E)$ and vertical $Diss_{ver}(E)$ dissipation. PE changes in time due to the advection of PE $Adv(P)$, the horizontal $Diff_{hor}(P)$ and vertical $Diff_{ver}(P)$ turbulent diffusion, and the diffusion of PE through the surface due to fluxes of heat and salt $Fluxes$. The exchange between KE and PE is characterized by the magnitude and sign of the buoyancy work. If the buoyancy work has positive value, then PE is converted to KE.

Let us consider the integral components which were averaged over the year. Note that some results of intra-annual energetics analysis were published earlier in Demyshev and Dymova (2016) for 2006 and Demyshev and Dymova (2017)) for 2011. But here we compare these data to estimate the influence of interannual variability on the energetics and the circulation regime of the Black Sea. Diagrams of the energy balance for 2006 and 2011 are presented in Fig. 5. The left side of the diagram describes the balance of KE, while the right side describes the balance of PE, and all values are given as density of energy flux (10^{-7} W m^{-3}). KE and PE are decreased in 2006 (Fig. 5a). The inflow in KE as a result of the wind stress work and the buoyancy work is less than the contribution due to horizontal and vertical dissipation. The main balance is observed between the energy inflow from the wind and the vertical turbulent mixing. The contributions of the advective components in the KE budget are small, but they are not zero due to nonzero momentum flows through the river mouths and straits. PE averaged over 2006 is decreased due to the difference between the buoyancy work and term of $Diff_{ver}(P)$. The vertical turbulent diffusion consists of four components:

$$\begin{aligned} Diff_{ver}(P) &= Diff_{ver}^{in}(P) + Diff_{ver}^{\rho}(P) + Diff_{ver}^{\kappa_V}(P) \\ &\quad + Diff_{ver}^{add}(P). \end{aligned} \qquad (4)$$

The first and the fourth terms in Eq. (4) are three orders smaller than the second and the third terms, so further on, we neglect $Diff_{ver}^{in}(P)$ and $Diff_{ver}^{add}(P)$. The analysis of the temporal variability of the second and the third terms of Eq. (4) shows that they compensate each other and their difference determines the rate of PE change for both years. In 2006, the total contribution of the second and the third terms of Eq. (4) was small. In 2011, $Diff_{ver}(P)$ has grown mainly due to an increase in $Diff_{ver}^{\rho}(P)$.

The directions of energy fluxes remained unchanged in 2011, but we observe a quantitative difference in contrast to 2006. The main effect is an increment of the year-mean rate of KE and PE change (Fig. 5b). It means the accumulation of circulation energy. The general contribution to the KE change gives the difference between the wind stress work and the vertical turbulent mixing, same as in 2006. The values of $Diss_{ver}(E)$ and the buoyancy work decreased by 1.65 and 2

Fig. 5 Diagrams of the magnitudes (10^{-7} W m^{-3}) and directions of the KE and PE budget components: **a** 2006 and **b** 2011
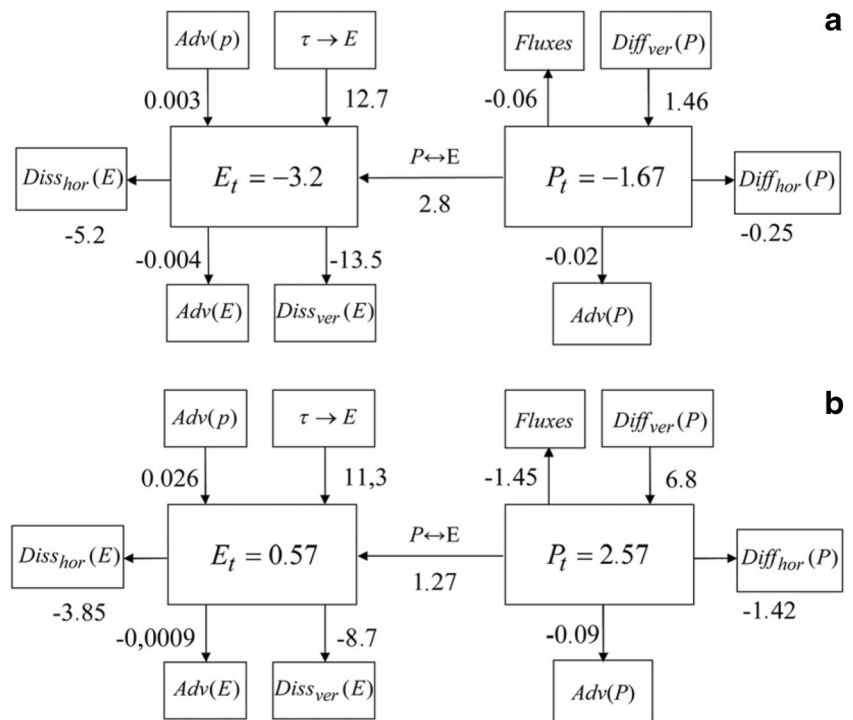
times, respectively, compared to 2006. It leads to the growth of the year-mean KE in 2011. The growth of PE in 2011 is due to the following processes. The year-mean value of $Diff_{ver}(P)$ is more than four times higher in contrast to 2006 and the main contribution here belongs to $Diff_{ver}^{\rho}(P)$. The buoyancy work is more than twice lower in comparison with 2006. As a result of the horizontal diffusion influence and the release of heat into the atmosphere, the energy decreased but the term $Diff_{ver}^{\rho}(P)$ led to the growth of PE in 2011.

To estimate the seasonal variability of the KE and PE budget components, we consider the terms of Eqs. (1) and (2), which were averaged over each season. We allocate hydrological seasons as 3-month periods beginning on January 1, April 1, July 1, and October 1. The most significant contributions to the energy budget on a seasonal scale give the wind stress work, the buoyancy work, the vertical dissipation, and the vertical diffusion for 2006 and 2011 years. The values and signs of these components of energy balance for 2006 and 2011 are presented in Table 1. The sign "minus" means that this term decreases the energy. Comparison of modeling data for 2006 and 2011 shows that there is only one difference in the signs. $Diff_{ver}(P)$ is positive in winter 2006, while it is negative in winter 2011. The possible reason is an increase in $Diff_{ver}^{\rho}(P)$ contribution, which led to an enhanced total vertical diffusion flux in the winter of 2006. Most likely, this effect is associated with the choice of boundary conditions: an impact of storm winds in the winter of 2006 induced more intensive vertical mixing, cooling of the upper mixed layer and increase in its density.

In winter and autumn of both 2006 and 2011, the energy inflow from the wind is mainly compensated by the work due to vertical friction. In spring, the integral flows are not so significant and KE is formed by the balance between the buoyancy work, work due to the vertical dissipation, and the energy inflow from the wind. In summer of 2011, the energy inflow from the wind decreased: $3 \cdot 10^{-7}$ W m^{-3} in contrast to $8.3 \cdot 10^{-7}$ W m^{-3} for 2006. The KE outflow due to the vertical dissipation decreased too. Table 1 shows that the contribution of the wind stress work exceeds outflow of KE due to the vertical dissipation in all seasons of 2011. However, in spring and summer of 2006, the KE reduction due to vertical friction

Table 1 Integral components of KE and PE budgets (10^{-7} W m^{-3}) averaged over all seasons of 2006 and 2011

	$\tau \rightarrow E$	$P \leftrightarrow E$	$Diss_{ver}(E)$	$Diff_{ver}(P)$	Fluxes
2006					
Winter	26.4	2.02	−25.9	0.32	−1.96
Spring	1.7	4.8	−4.5	4.5	1.3
Summer	8.3	2.3	−10.2	3.3	1.8
Autumn	14.4	2.04	−13.9	−2.3	−1.2
2011					
Winter	18.9	0.3	−14.5	−2.3	−1.9
Spring	6	1.8	−3.7	13.8	1
Summer	3	2.6	−2.5	15.6	1.4
Autumn	17.6	0.7	−12.1	−0.2	−2.1

Terms correspond to Eqs. (1) and (2)

is greater than its increase from the wind. Maybe a relaxation of the system after storm winds in winter of 2006 took place, since the number and intensity of storms in winter of 2011 were lower according to the SKIRON data.

The biggest difference in the PE energy budget formation is observed in the magnitude of work due to the vertical turbulent diffusion in the warm season. In spring of 2011, the value $Diff_{ver}(P)$ reaches $13.8 \cdot 10^{-7}$ W m^{-3}, and in summer of 2011, it increases to $15.6 \cdot 10^{-7}$ W m^{-3}. On average, over the spring-summer period of 2011, the absolute value of $Diff_{ver}(P)$ increased by 1.44 times and the value of $Diff_{ver}^{\kappa_V}(P)$ is increased by 1.23 times, both compared to 2006. In May, July, and September of 2011, intensive fluctuations of mean values of $Diff_{ver}^{\kappa_V}(P)$ and $Diff_{ver}^{\rho}(P)$ are observed. Apparently, such variability was caused by the inhomogeneity of the density field due to the development of mesoscale eddies in the central part of the sea (as will be shown below in Fig. 8e). The analysis showed that the ratio of relative contributions of $Diff_{ver}^{\rho}(P)$ and $Diff_{ver}^{\kappa_V}(P)$ into the magnitude of full vertical diffusion work is changed in 2011, if compared to 2006: 55.49 and

44.51% (Fig. 6b) against 51.68 and 48.32% (Fig. 6a), respectively. As you see in Fig. 6, the term $Diff_{ver}^{\rho}(P)$ is more energy-significant for both experiments; however, the relative decrease in the term $Diff_{ver}^{\kappa_V}(P)$ contribution leads to an increase in the contribution to the PE change due to vertical diffusion.

Since the contribution of $Diff_{ver}(P)$ to the year-mean value of P_t is the largest, it is highly important to have the heat and salt fluxes from the atmosphere with minimal errors and to take them into account accurately in the boundary conditions. The second condition for reduction of the forecasting error is correct parameterization of sub-grid processes. In our experiments, we used the Mellor-Yamada turbulence closure model, but the question remains open: which of the existing turbulence closure models (Pacanowski and Philander 1981; Mellor and Yamada 1982; Rodi 1987; Large et al. 1994) is more preferable?

The ocean energy cycle is formed by four energy reservoirs, which describe the kinetic energy E_m and the available potential energy P_m of the time-mean circulation, as well as
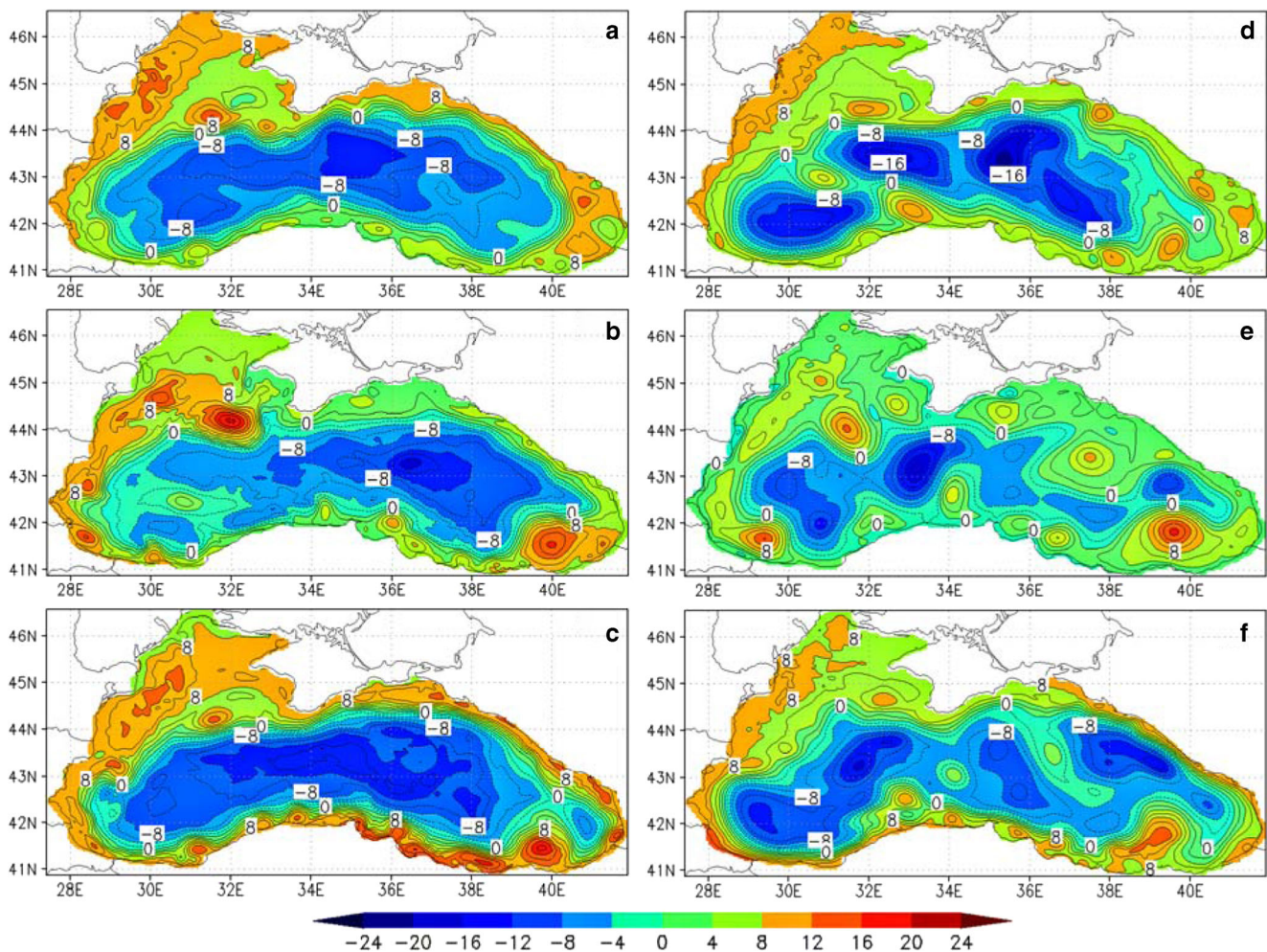

Fig. 8 Modeling sea level (cm) fields: **a** May 15, 2006; **b** September 15, 2006; **c** November 15, 2006; **d** May 15, 2011; **e** September 15, 2011; and **f** November 15, 2011

the kinetic energy E_e and the available potential energy P_e of the time-varying circulation (Von Storch et al. 2012) associated with the mesoscale variability. Here and hereafter, the indices m and e indicate mean current energy and eddy energy, respectively. We should remind that the results for the energy of the Black Sea circulation presented above are derived from solving Eqs. (1) and (2), which correspond exactly to the equations of the hydrodynamics model. However, since we calculate the energy equations at the same time steps as the model equations, we are not able to immediately derive eddy energy components as deviations from the mean value. Therefore, the output model data obtained for each day of 2006 (Exp.1) and for each day of 2011 (Exp.2) were averaged over the years. For the estimation of eddy fluxes, we used the fluctuations of the velocity components and the density from their time-mean values:

$$x' = x - \overline{x}.$$

The overbar denotes time-averaged values, and the prime denotes the deviation from the respective time-mean. The deviation square was calculated as:

$$\overline{x' \cdot y'} = \overline{x \cdot y} - \overline{x} \cdot \overline{y}.$$

To calculate the integral values of the energy reservoirs and the rates of energy conversion between them, we used the relations (1)–(4) and (14)–(17) from Von Storch et al. (2012). The integration was carried out over the upper 200-m layer, because below the changes of velocities and density are insignificant. We also calculated integral contributions characterizing the sources of the eddy energy and the mean current energy. The time-varying wind stress τ_e and the time-varying heat and salt fluxes from atmosphere $Fluxes_e$ are the sources E_e and P_e, respectively.

Let us consider the year-mean energy cycles of the Black Sea in 2006 and 2011. Figure 7 presents diagrams of the year-mean integrals of energy reservoirs and rates of energy conversion for two experiments. $C(X,Y)$ denotes the rate of conversion between X and Y: if $C(X,Y) > 0$, then X converts to Y and vice versa. The values are given in the following units: $EJ = 10^{18}$ J, $PJ = 10^{15}$ J, and $GW = 10^9$ W. As can be seen from Fig. 5, the contributions of E_m and E_e to the total KE of the Black Sea circulation are differed for Exp.1 and Exp.2: the contribution of E_m prevailed in 2006, but the contribution of E_e prevailed in 2011. The contribution of E_e to the total KE is 38% in Exp.1 and 62% in Exp.2. The KE change was provided by the wind stress work. At the same time, energy generation due to τ_m and τ_e had similar magnitudes in 2006, but in 2011, τ_e increased by more than three times and τ_m weakened. E_e was also replenished by the flux $C(E_m, E_e)$, which was associated with the barotropic instability of the mean current. It was the most energetically relevant flux exceeding the year-mean value of τ_e several times for both experiments. Thus, the eddies were developed mainly due to barotropic instability of the mean current in 2006 and 2011. E_m was nourished by the contributions of the wind stress work and by the conversion $P_m \rightarrow E_m$, which was described by the buoyancy work. These fluxes were comparable in both experiments. The exchange between the E_e and P_e was an order of magnitude smaller than the similar flux for the mean current. The year-mean energy transferred from E_e to P_e in both experiments. P_e was nourished due to the heterogeneity of the atmosphere flux, while year-mean P_m decreased due to the transfer of energy into the atmosphere in both experiments. Analysis of the spatial distribution of the eddy energy sources (maps are not presented here) showed that in 2006 the greatest contributions were observed near the Western coast, near the Kerch Peninsula, and the Anatolian coast; in 2011, only near the Western coast. The areas of greatest contributions $Fluxes_e$
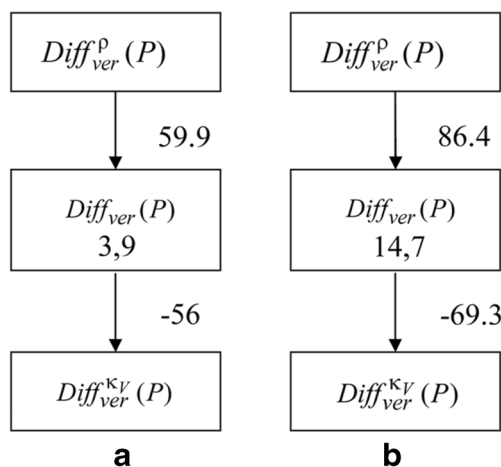

Fig. 6 Diagrams of main components of the vertical diffusion PE (10^{-7} W m^{-3}): **a** 2006, **b** 2011
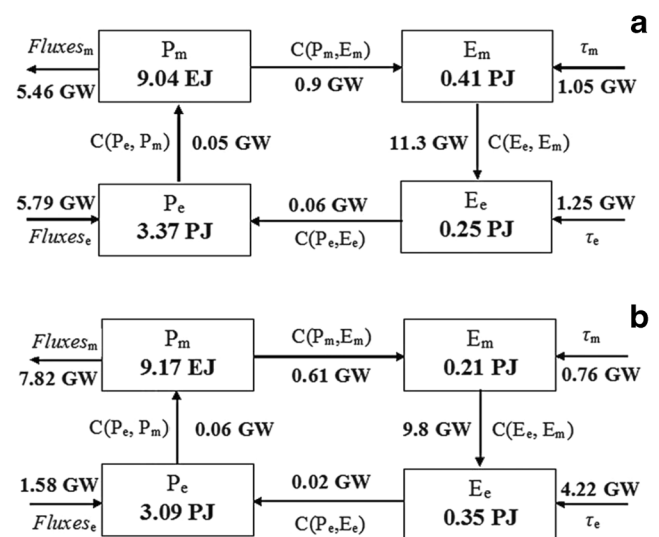

Fig. 7 The Black Sea energy cycles in 2006 (**a**) and 2011 (**b**). Energy reservoirs are in exajoules (EJ, 10^{18}) and petajoules (PJ, 10^{15}) and rates of generation and conversion are in gigawatts (GW, 10^9)

were located in the Northern part of the sea, near the Eastern coast of Crimea, and in the North-Western Shelf for both experiments.

It is important to note that we do not demonstrate the rate of dissipation of eddy energy and mean current energy in Fig. 7. According to the analogy of Von Storch et al. (2012), these components are calculated algebraically from the equations of energy budget. However, Fig. 5 shows that the year-mean budget can be negative or positive. Therefore, to avoid underestimation or overestimation of the energy dissipation rate, it is necessary to introduce eddy analogues for dissipative and diffusive components of the right parts of Eqs. (1) and (2) and calculate them directly. We plan to carry out this work in the future.

5.2 Circulation

Analysis of the modeling results allowed us to identify two regimes of variability of the Black Sea circulation. We demonstrate these on the example of 2006 and 2011. In 2006, the basin was covered by a large-scale cyclonic gyre (Fig. 8a–c). In this circulation model, the mesoscale eddies with the sizes of the order of 10 km were formed and intensively developed between the Rim Current and the shore (Fig. 8c). They hardly penetrated into the abyssal part of the sea, since the Rim Current prevented their movement. The mesoscale eddies were sometimes generated in the central part of the sea, when the circulation had a complex irregular structure (Fig. 8b). In 2011, the Black Sea circulation looked like a set of several mesoscale eddies (Fig. 8d, e), which merged into a single cyclonic gyre only at the end of the year (Fig. 8f). Energy analysis showed that the contribution of the wind stress work during the cold season of 2011 decreased by 35% on average compared to 2006. This led to a decrease in inflow to the KE of circulation and weakening of the Rim Current. As a result, the extensive cyclonic gyre broke down into three mesoscale eddies (Fig. 8d). Therefore, the mesoscale eddies were observed not only in the coastal zones but also formed along the periphery of large cyclonic gyres during 2011 (Fig. 8d, e). In contrast to 2006, the coastal eddies could be moving to the central part of the sea transferring mass, heat, and energy. Thus, the sub-basin and mesoscale variability of the Black Sea circulation can be significantly different from year to year.

5.3 Mesoscale variability

As shown in Section 3, well-known mesoscale SA and BA are reproduced in the simulated velocity fields. The analysis of the spatial distribution of the buoyancy work showed that its absolute values were the highest in the eddy location zones. Figure 9a presents the fragments of the velocity field for the period of the formation and evolution of the SA from July till October 2006. We also calculated the time variations of

volume integrals of E_e (Fig. 10a), $C(E_e,E_m)$, and $C(P_e,E_e)$ (Fig. 10b) in the Sevastopol domain for this period. The domain is bounded by meridians of 31° E and 34° E, parallels of 43.5° N and 45° N, vertically from the surface to the depth of 200 m. We should remind that the energy conversion from E_m to E_e happens due to the barotropic instability and the energy conversion between P_e and E_e is associated with the baroclinic instability.

Let us consider the process of the SA development. The eddy arose quasi-periodically with an interval of about 3 months. In the beginning, the eddy with the size of about 60 km detached itself from the edge of the Crimean Peninsula (Fig. 9a, June 22). For about of a month, the kinetic energy of the Rim Current was gradually increasing the velocity in the anticyclone. The eddy captured denser water from the abyssal sea part and transported it to the coastal part due to orbital velocities. The water downwelling in the eddy center and upwelling along the eddy periphery are intensified (Fig. 9b). As a result, the energy inflow to the available P_e was provided. It is clear in Fig. 10b: the negative value of $C(P_e,E_e)$ prevails on August 12–28 and the value $C(E_e,E_m)$ periodically changes a sign. Increases in $C(P_e,E_e)$ and $|C(E_e,E_m)|$ (modulus of $C(E_e,E_m)$) were both observed after August 26, that points out the enhancement of the barotropic and the baroclinic instability processes. The eddy had already reached the size of 170 km along the long axis and the mean velocity had increased to 40 cm/s (Fig. 9a, August 26). Later, the E_e increased significantly (Fig. 10a) and the eddy was intensified (Fig. 9a, September 21). When the E_e reached maximum values of $7.18 \cdot 10^{13}$ J, then the $|C(E_e,E_m)|$ exceeded $C(P_e,E_e)$ more than five times. The SA began to move toward the South-West along the periphery of the Rim Current due to the formation of a meander. The E_e decreased (Fig. 10a), the flux of $C(E_e,E_m)$ weakened, and the flux of $C(P_e,E_e)$ increased (Fig. 10b) as the anticyclone was leaving the selected domain. Note that the τ_e does not have a clear effect on the temporal variability of E_e. A new eddy was formed toward the West from Crimea by the end of the time interval. The newly formed eddy was getting stronger for the next several days and finally a new Sevastopol anticyclone was generated. Then, the process repeated. Thus, the generation of the SA in summer 2006 was conditioned by both barotropic and baroclinic instabilities but later the evolution of the SA and its E_e were associated with barotropic instability during the most intensive development phase.

The BA was formed in end of spring from a weak anticyclonic eddy with center located in point 41° E, 41.5° N (Fig. 8a), and the mechanism of its formation was associated with the influence of mesoscale anticyclones coming from the Anatolian coast (Staneva et al. 2001). It was observed throughout the year, enhancing and weakening from time to time (Fig. 8b). Enhancing of the BA happened because of the formation of smaller eddies, their transfer along the Anatolian
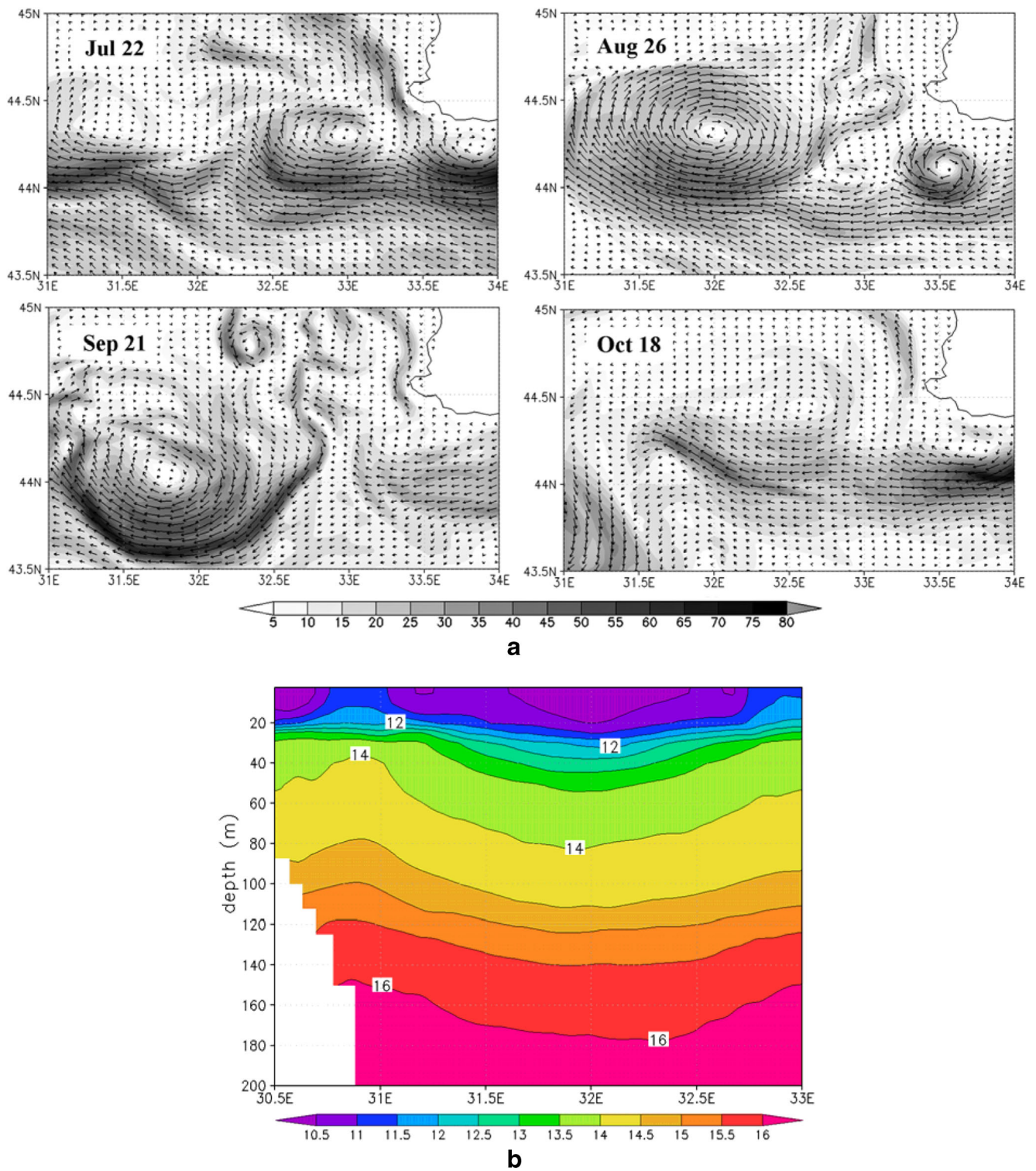
Fig. 9 Fragments of the current velocity (cm/s) fields (**a**) and conditional density on the zonal transect (30.5–33° E, 44.3 °N) on August 26, 2006 (**b**) in the Sevastopol anticyclone area

coast, and finally merging with the anticyclone. In autumn, two eddies of cyclonic and anticyclonic vorticity were located in the South-Eastern corner of the basin (Fig. 8c). In December, a quite strong anticyclone was formed again.

There was more complex dynamics in 2011. The SA was also formed quasi-periodically but it was weaker. The SA could have moved to the central part of the sea in 2011 (Fig. 8d, e), since the basin-scale dynamics consisted of three

Fig. 10 Volume integrals of E_e (**a**), the rates of conversion $C(E_e,E_m)$ and $C(P_e,E_e)$, and τ_e (**b**) in the Sevastopol anticyclone area during the evolution period of the Sevastopol anticyclone
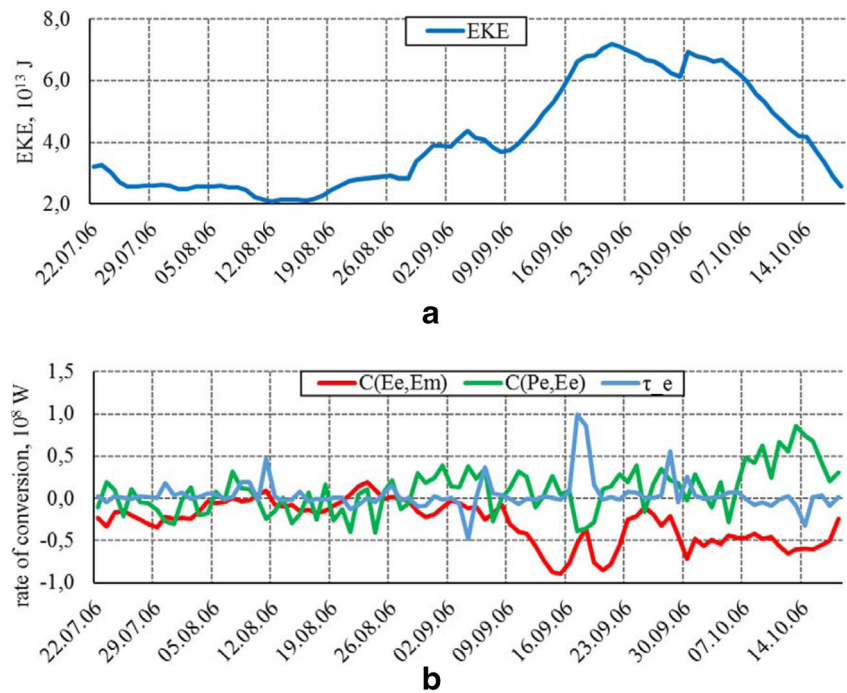

large-scale eddies. The behavior of the SA became similar to its evolution in 2006 after the cyclonic eddies had merged into a general gyre (Fig. 8f). The BA existed during all the 2011. In spring, it shifted to the west probably due to the structure of the main circulation (Fig. 8d). The generation of mesoscale eddies along the Anatolian coast was more intensive in contrast to 2006. These mesoscale eddies moved along the periphery of the Rim Current and merged with the BA, thereby determining its evolution (Fig. 8f).

The intensive coastal mesoscale eddy formation was observed near the Anatolian, Caucasian, and Crimean coasts between the Rim Current and shore over the continental slope. The Rim Current flowed around the irregularities in the shoreline in these areas which led to the formation of coastal mesoscale eddies due to the vertical velocity shift (Dymova 2017) for both experiments. We provide the development of eddies near the Anatolian coast as an example of this process (Fig. 11a, c). They were formed quasi-periodically; their lifetime was about 20 days on average. The eddies had the size of about 15–20 km and were about 100-m deep. In accordance with the ratio (3), the Rossby number was varied from 0.2 to 0.6 in these circulation zones, so we classified the mentioned eddies as mesoscale. Spatial distribution maps of the buoyancy work (Fig. 11b, d) pointed out the process of development of the Rim Current instability in the zones where the coastal eddies were located. The mesoscale eddies transported denser waters from the coastal zone and gradients in the density field between their center and periphery increased. The largest magnitudes of the buoyancy work modulus were observed here, which indicated intensive conversion between KE and PE.

A similar situation was observed during the formation of eddies near the Crimean and Caucasian coasts (Fig. 12a, c). Here, their size reached about 10 km and the eddies were 30–60 m deep. Magnitudes of parameters (3) for the considered zones allowed us to prove that the eddies, which had been registered between 44° N and 46° N in the Black Sea, had mesoscale characteristics. As seen in Fig. 12b, d, the generation of these mesoscale eddies was accompanied by the intensive exchange between KE and PE which was described by the buoyancy work.

To estimate the contributions of baroclinic and barotropic instabilities into the mesoscale eddy generation, we calculated the volume integrals of E_e, $C(E_e,E_m)$, and $C(P_e,E_e)$ during all year near the Anatolian, Crimean, and Caucasian coasts for both experiments. In the northern sea part, the domain is bounded by meridians of 33° E and 40° E, parallels of 44.3° N and 45.3° N, and in the southern sea part, the domain is bounded by meridians of 34° E and 39° E, parallels of 40.8° N and 42.5° N. Integration was carried out from surface to the horizon of 100 m for both domains. The next results are obtained for Crimean and Caucasian coasts. In the first half of 2006, the contribution of $|C(E_e,E_m)|$ exceeds in two times value of $C(P_e,E_e)$ and the E_e is also more in two times than the E_e in the second half of 2006. In the second half of 2006, contribution into the E_e due to $C(P_e,E_e)$ is increased in 6.5 times and correspondence between biggest values of E_e and $C(P_e,E_e)$ is observed. The processes of baroclinic instability prevail until the end of 2006. The growth of E_e is revealed in the cold seasons of 2011 due to increase both $|C(E_e,E_m)|$ and $C(P_e,E_e)$. In spring and summer, the maximum value of $C(P_e,E_e)$ exceeds the $|C(E_e,E_m)|$ more than in seven times.

Fig. 11 Fragments of the sea level (cm) fields and the buoyancy work (10^{-7} W m^{-3}) fields at the depth of 20 m: **a**, **c** November 19, 2006 and **b**, **d** October 26, 2011
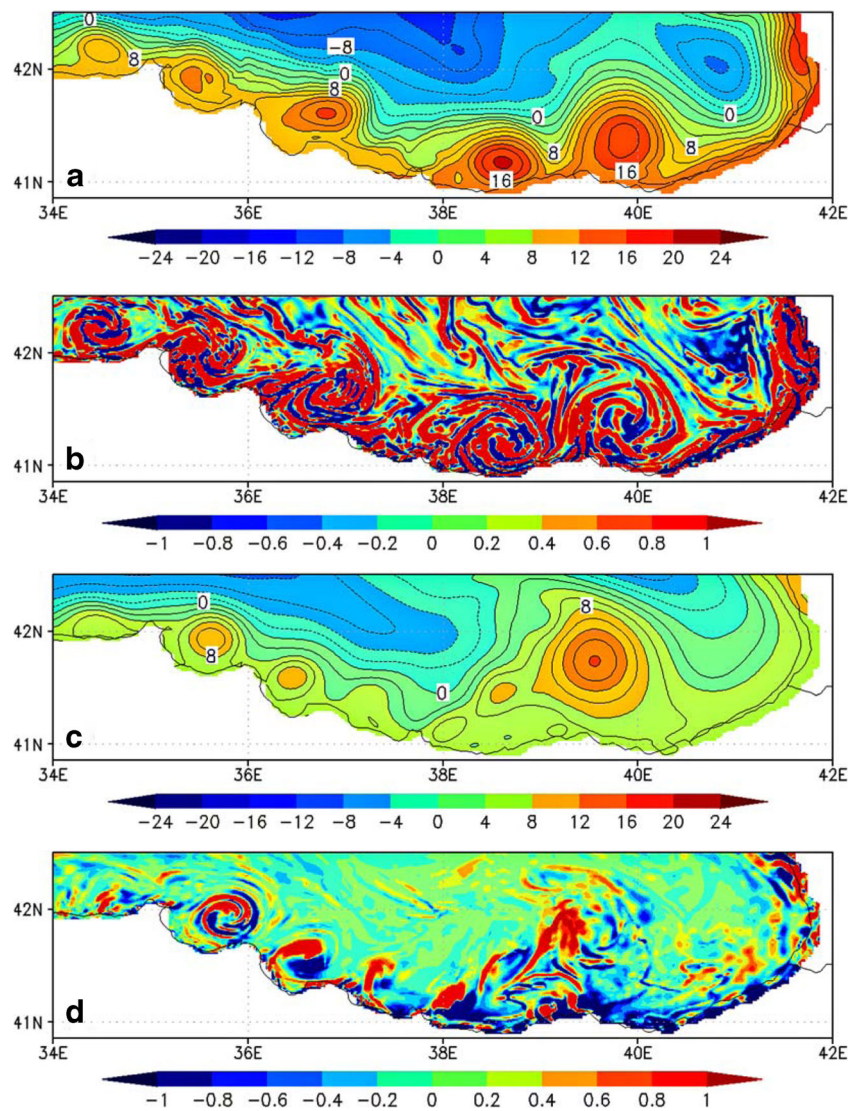
Analysis of energy fluxes near the Anatolian coast is shown that E_e in winter and autumn of 2006 is bigger in four times than in spring and summer. Herewith the contributions of barotropic and baroclinic instabilities into the eddy generation in winter and autumn are approximately identical. In summer of 2006, the $C(P_e,E_e)$ exceeds the $|C(E_e,E_m)|$ in 1.5–2 times. The fluxes of $C(E_e,E_m)$ and $C(P_e,E_e)$ give almost equal contributions into the E_e from January till September 2011. Starting from October 2011 the value of $C(P_e,E_e)$ is increased in 3.5 times. The growth of $C(P_e,E_e)$ led to increase of the E_e in three times compared to period from January till September.

Let us consider year-mean volume integrals of the $C(P_e,E_e)$ and the $C(E_e,E_m)$ calculated in aforecited domains for the Anatolian, Crimean, and Caucasian coasts. The magnitudes and directions of these energy fluxes are presented in Fig. 13. As seen, the year-mean values of $C(P_e,E_e)$ and the $C(E_e,E_m)$ near the Crimean and Caucasian coasts (Fig. 13a) are comparable to each other for both experiments. The

conversion rates $C(P_e,E_e)$ are less than $C(E_e,E_m)$ near the Anatolian coast in 2006 and 2011 (Fig. 13b). Note that E_e in both domains are increased due to the barotropic and baroclinic instabilities in 2011 and only due to the barotropic instability in 2006. As was shown in Section 5.2, the Rim Current was more intensive in 2006 compared to 2011.

6 Conclusion

The hydrological and energetic features of the Black Sea in 2006 and 2011 were reconstructed using the numerical model. The annual and seasonal fields of the current velocity, density, and components of the kinetic and potential energy of circulation were calculated to estimate the scales, the reasons, and mechanisms of the spatial-temporal variability of the Black Sea circulation. The eddy energy was studied in order to investigate the mesoscale variability.
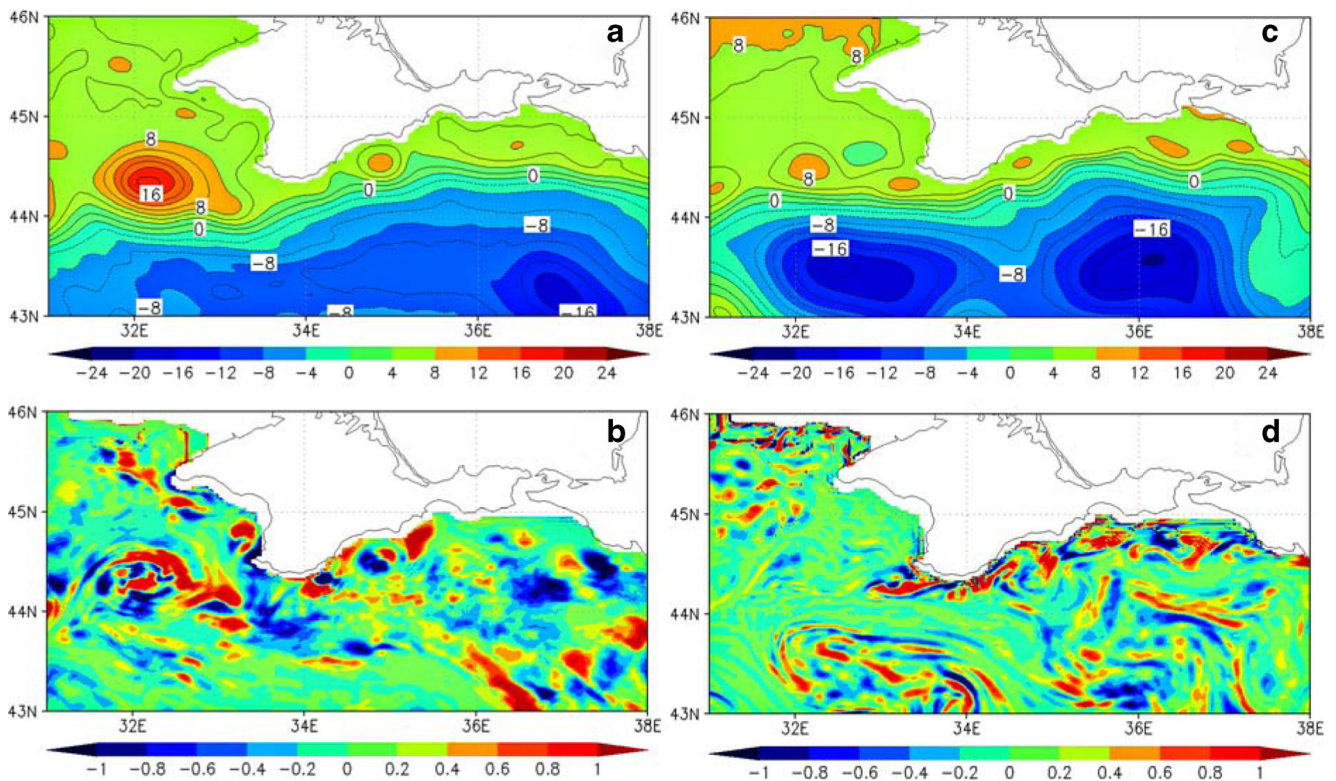
Fig. 12 Fragments of the sea level (cm) fields (top panel) and the buoyancy work (10^{-7} W m^{-3}) fields at the depth of 20 m (bottom panel): **a, c** August 13, 2006 and **b, d** May 1, 2011

Comparative energy analysis showed that the main components of the annual and seasonal budgets of kinetic and potential energies of circulation were the works due to wind action, turbulent mixing, and vertical diffusion. It means that accurate parameterization of sub-grid processes is essential to reduce modeling errors. We performed estimates of the time-mean and time-varying circulation energies, which were associated with the mean current energy and eddy energy, respectively. The year-mean cycle of energy conversion between the mean current and the eddies in 2006 and 2011 was described. The

sources of eddy KE were the flux of KE from the currents to eddies and the time-varying wind. The eddy PE increased due to the time-varying component of the heat and salt flux from the atmosphere. It was discovered that an increase in the time-varying wind stress work with the weakening of the time-mean wind stress in 2011 led to an increase in eddy KE. The analysis of the energy conversion rates showed that the most energy-efficient flux was the transport of KE from the mean current to the eddies, which was associated with the barotropic instability. The value of the flux describing the rate of conversion between the KE and PE of the mean current was an order of magnitude less. The year-mean transport of the eddy available PE by pathway $E_e \rightarrow P_e \rightarrow P_m$ was minimal in both experiments. Note that the direction of the eddy available PE year-mean flux integrated over basin is different from analogical fluxes integrated over some coastal zones. So the transported from the eddy available PE to the eddy KE which is associated with baroclinic instability was observed near the Anatolian, Crimean, and Caucasian coasts in 2011.

The modeling results reproduced the complex mesoscale variability of the Black Sea circulation. It was shown that the character of variability essentially depends on the mode of general circulation, which is determined by the integral action of wind in winter. The experimental data for 2006 demonstrated the well-known structure of currents in the Black Sea but the basin-scale circulation in 2011 led to a qualitatively different dynamics of mesoscale eddies. The main difference was
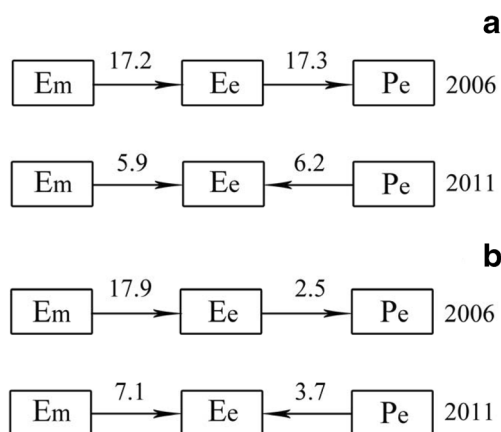

Fig. 13 Year-mean volume integrals of $C(E_e, E_m)$ and $C(P_e, E_e)$ for the Crimean and Caucasian coast (**a**) and the Anatolian coast (**b**) in 2006 and 2011. The conversion rates are in megawatts (MW, 10^6)

the ability of eddies to move freely into the abyssal part of the basin. They provided the exchange of mass, heat, and salt between the coastal zones, where seawater is fresher and warmer, and the abyssal part.

The mechanism of development and intensification of the coastal mesoscale eddies was implemented as follows. The meanders in the Rim Current structure were generated due to flowing around the shoreline irregularities. They supplied the coastal low-powered eddies with the KE. The orbital velocities of eddies increased and, as a result, denser waters were involved into the coastal zone and less dense water—into the deep part of the sea. Thus, the horizontal density gradient increased and the available PE of eddy grew as well. Analysis of the energy fluxes between the mean current KE and the eddy KE and between the eddy available PE and the eddy KE in coastal zones showed that variability of the eddy KE in the Black Sea mainly depends on common basin-scale circulation structure. If the coastal currents are intensive, so the mesoscale coastal eddy generation is associated with barotropic instability. When the coastal currents are weak, then the mesoscale coastal eddy generation is due to both barotropic and baroclinic instabilities.

References

Cessi P, Pinardi N, Lyubartsev V (2014) Energetics of semienclosed basins with two-layer flows at the strait. J Phys Oceanogr 44:967–979. https://doi.org/10.1175/JPO-D-13-0129.1

Chelton DB (2001) Overview of the high-resolution ocean topography science working group meeting. In: Chelton DB (ed) Report of the high-resolution ocean topography science working group meeting. Oregon State University, Corvallis, pp 1–19

Chen G, Wang D, Hou Y (2012) The features and interannual variability mechanism of mesoscale eddies in the Bay of Bengal. Cont Shelf Res 47:178–185. https://doi.org/10.1016/j.csr.2012.07.011

Cushman-Roisin B, Korotenko KA, Galos CE, Dietrich DE (2007) Simulation and characterization of the Adriatic Sea mesoscale variability. J Geophys Res 112:C03S14. https://doi.org/10.1029/2006JC003515

Demyshev SG (2004) Energy of the Black Sea climatic circulation. 1. Discrete equations of the time rate of change of kinetic and potential energy. Meteorol Gidrol 9:65–80

Demyshev SG (2012) A numerical model of online forecasting Black Sea currents. Izv. Atmos. Ocean. Phys. 48(1):120–132. https://doi.org/10.1134/S0001433812010021

Demyshev SG, Dymova OA (2016) Analyzing intraannual variations in the energy characteristics of circulation in the Black Sea. Izv Atmos Ocean Phys 52(4):386–393. https://doi.org/10.1134/S0001433816040046

Demyshev SG, Dymova OA (2017) Numerical analysis of the Black Sea energy budget in 2011. IOP Conf Series Journal of Physics Conf Series 899(2):022004. https://doi.org/10.1088/1742-6596/899/2/022004

Demyshev SG, Ivanov VA, Markova NV (2009) Analysis of the Black-Sea climatic fields below the main pycnocline obtained on the basis of assimilation of the archival data on temperature and salinity in the numerical hydrodynamic model. Phys Oceanogr 19(1):1–12. https://doi.org/10.1007/s11110-009-9034-x

Demyshev S, Knysh V, Korotaev G, Kubryakov A, Mizyuk A (2010) The MyOcean Black Sea from a scientific point of view. Mercator Ocean Quarterly Newsletter 39:16–24

Dymova O (2017) High-resolving simulation of the Black Sea circulation. 13th International MEDCOAST Congress on Coastal and Marine Sciences, Engineering, Management and Conservation, MEDCOAST 2017. 2:1203-1213

Farda A, Déué M, Somot S, Horányi A, Spiridonov V, Tóth H (2010) Model ALADIN as regional climate model for Central and Eastern Europe. Stud Geophys Geod 54(2):313–332. https://doi.org/10.1007/s11200-010-0017-7

Gill AE (1982) Atmosphere-ocean dynamics. Academic Press, Orlando

Ginzburg AI, Kostianoy AG, Nezlin NP, Soloviev DM, Stanichny SV (2002) Anticyclonic eddies in the northwestern Black Sea. J Mar Syst 32:91–106. https://doi.org/10.1016/S0924-7963(02)00035-0

Ibraev RA, Trukhchev DI (1996) A diagnosis of the climatic seasonal circulation and variability of the cold intermediate layer in the Black Sea. Izv Atmos Ocean Phys 32(5):604–619

Kallos G, Nickovic S, Papadopoulos A, Jovic D, Kakaliagou O, Misirlis N, Boukas L, Mimikou N, Sakellaridis G, Papageorgiou J, Anadranistakis E, Manousakis M (1997) The regional weather forecasting system SKIRON: an overview. Proceedings of the International Symposium on Regional Weather Prediction on Parallel Computer Environments, (15–17 October 1997). pp 109-122. Athens, Greece

Kersalé M, Doglioli AM, Petrenko AA (2011) Sensitivity study of the generation of Hawaii mesoscale eddies. Ocean Sci 7:277–291. https://doi.org/10.5194/os-7-277-2011

Khaliulin AK, Godin EA, Ingerov AV, Zhuk EV, Galkovskaya LK, Isaeva EA (2016) Ocean data bank of the Marine Hydrophysical Institute: information resources to support research in the Black Sea coastal zone. Ecol Saf Coast Shelf Zones of the Sea 1:89–95 (in Russian)

Kjellsson J, Zanna L (2017) The impact of horizontal resolution on energy transfers in global ocean models. Fluids 2(3):45. https://doi.org/10.3390/fluids2030045

Korotenko KA (2015) Modeling mesoscale circulation of the Black Sea. Oceanology 55:820–826. https://doi.org/10.1134/S0001437015060077

Kortcheva A, Dimitrova M, Galabov V (2009) A wave prediction system for real time sea state forecasting in Black Sea. Bulgarian J Meteorology and Hydrology 1:1–16

Kubryakov AA, Stanichny SV (2015a) Seasonal and interannual variability of the Black Sea eddies and its dependence on characteristics of the large-scale circulation. Deep-Sea Res I Oceanogr Res Pap 97:80–91. https://doi.org/10.1016/j.dsr.2014.12.002

Kubryakov AA, Stanichny SV (2015b) Dynamics of Batumi anticyclone from satellite data. Phys Oceanogr 2:59–68. https://doi.org/10.22449/0233-7584-2015-2-67-78 http://physical-oceanography.ru/repository/2015/2/en_201502_06.pdf

Large WG, McWilliams JC, Doney SC (1994) Oceanic vertical mixing: a review and a model with a nonlocal boundary layer parameterization. Rev Geophys 32(4):363–403. https://doi.org/10.1029/94RG01872

Liang J-H, McWilliams JC, Kurian J, Colas F, Wang P, Uchiyama Y (2012) Mesoscale variability in the northeastern tropical Pacific: forcing mechanisms and eddy properties. J Geophys Res 117:C07003. https://doi.org/10.1029/2012JC008008

Mamaev ON (1963) Oceanographic analysis in the system a-S-T-p. Moscow State University Publishing, Moscow (in Russian)

Mellor GL, Yamada T (1982) Development of a turbulence closure model for geophysical fluid problems. Rev Geophys 20(4):851–875. https://doi.org/10.1029/RG020i004p00851

Menna M, Poulain P-M (2014) Geostrophic currents and kinetic energies in the Black Sea estimated from merged drifter and satellite altimetry data. Ocean Sci 10:155–165. https://doi.org/10.5194/os-10-155-2014

Motyzhev SV, Tolstosheev AP, Lunev EG, Bayankina TM, Litvinenko SR, Cryl MV, Yurkevich NYu, Mikhailova NV (2016) Database of the operational drifter observations for the Black Sea region. Certificate of state registration #2016620404 from 01.04.2016

Oguz T, Malanotte-Rizzoli P, Aubrey D (1995) Wind and thermohaline circulation of the Black Sea driven by yearly mean climatological forcing. J Geophys Res 100(C4):6846–6865. https://doi.org/10.1029/95JC00022

Pacanowski RC, Philander SGH (1981) Parameterization of vertical mixing in numerical models of tropical oceans. J Phys Oceanogr 11:1443–1451. https://doi.org/10.1175/1520-0485(1981)011<1443:POVMIN>2.0.CO;2

Ponomarev VI, Fyman PA, Dubina VF, Ladychenko SY, Lobanov VB (2011) Mesoscale eddy dynamic over northwest Japan Sea continental slope and shelf (Simulation and remote sensing results). Curr Probl of Remote Sens Earth from Space 8(2):100–104 (in Russian)

Prants SV, Andreev AG, Uleysky MY, Budyansky MV (2017) Mesoscale circulation along the Sakhalin Island eastern coast. Ocean Dynamics 67:345–356. https://doi.org/10.1007/s10236-017-1031-x

Project "The Seas of the USSR" (1991) Hydrometeorology and hydrochemistry of the Seas of the USSR. In: Simonov AI, Altman EN (eds) Vol. 4: The Black Sea. Issue 1: Hydrometeorological conditions. St. Petersburg (in Russian)

Rachev N, Stanev E (1997) Eddy processes in semienclosed seas: a case study for the Black Sea. J Phys Oceanogr 27:1581–1601. https://doi.org/10.1175/1520-0485(1997)027<1581:EPISSA>2.0.CO;2

Rieck JK, Boning CW, Greatbatch RJ, Scheinert M (2015) Seasonal variability of eddy kinetic energy in a global high-resolution ocean model. Geophys Res Lett 42:9379–9386. https://doi.org/10.1002/2015GL066152

Robinson A, Harrison DE, Mintz Y, Semtner AJ (1977) Eddies and the general circulation of an idealized oceanic gyre: a wind and thermally driven primitive equation numerical experiment. J Phys Oceanogr 7:182–207. https://doi.org/10.1175/1520-0485(1977)007<0182:EATGCO>2.0.CO;2

Rodi W (1987) Examples of calculation methods for flow and mixing in stratified fluids. J Geophys Res 92(C5):5305–5328. https://doi.org/10.1029/JC092iC05p05305

Schaeffer A, Molcard A, Forget P, Frauníe P, Garreau P (2011) Generation mechanisms for mesoscale eddies in the Gulf of Lions: radar observation and modeling. Ocean Dynamics 61:1587–1609. https://doi.org/10.1007/s10236-011-0482-8

Shang X, Xu C, Chen G, Lian SM (2013) Review on mechanical energy of ocean mesoscale eddies and associated energy sources and sinks. J Tropical Oceanogr 2:24–36

Stanev EV (1990) On the mechanisms of the Black Sea circulation. Earth Sci Rev 28(4):285–319. https://doi.org/10.1016/0012-8252(90)90052-W

Staneva JV, Dietrich DE, Stanev EV, Bowman MJ (2001) Rim current and coastal eddy mechanisms in an eddy-resolving Black Sea general circulation model. J Mar Syst 31(1–3):137–157. https://doi.org/10.1016/S0924-7963(01)00050-1

Titov VB, Savin MT (2008) Spatial structure of the Black Sea current field. Russ Meteorol Hydrol 33:325–334. https://doi.org/10.3103/S1068373908050075

Trukhchev DI, Ivanov DV, Ibraev RA (1999) Current diagnosis over the "Diffuziya-84" test area at the western shelf of the Black Sea. Oceanology 39(4):474–482

Volcinger NE, Piaskovski RV (1968) Basic oceanological problems of the shallow water theory. Gidrometeoizdat, Leningrad

Von Storch J-S, Eden C, Fast I, Haak H, Hernndez-Deckers D, Maier-Reimer E, Marotzke J, Stammer D (2012) An estimate of the Lorenz energy cycle for the World Ocean Based on the 1/10° STORM/NCEP simulation. J Phys Oceanogr 42:2185–2205. https://doi.org/10.1175/jpo-d-12-079.1

Zatsepin AG, Kremenetskiy VV, Stanichny SV, Burdyugov VM (2010) Black sea basin-scale circulation and mesoscale dynamics under wind forcing In: Frolov, Resnaynsky (eds) Modern problems of ocean and atmosphere dynamics. Triada, Moscow, pp. 347–368. (in Russian).

Zhang Z, Zhao W, Tian J, Liang X (2013) A mesoscale eddy pair southwest of Taiwan and its influence on deep circulation. J Geophys Res Oceans 118:6479–6494. https://doi.org/10.1002/2013JC008994

Zhurbas VM, Zatsepin AG, Grigor'eva YV, Poyarkov SG, Eremeev VN, Kremenetsky VV, Motyzhev SV, Stanichny SV, Soloviev DM, Poulain P-M (2004) Water circulation and characteristics of currents of different scales in the upper layer of the Black Sea from drifter data. Oceanology 44(1):30–43